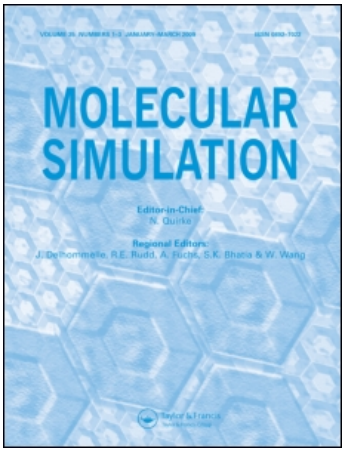


**Molecular Simulation**
Publication details, including instructions for authors and subscription information:
http://www.informaworld.com/smpp/title~content=t713644482

# Examination of structural stability and phase transitions in constant-pressure first-principles molecular dynamics simulations

Tetsuya Morishita; Shuichi Nosé

Online publication date: 03 June 2010

**To cite this Article** Morishita, Tetsuya and Nosé, Shuichi(2002) 'Examination of structural stability and phase transitions in constant-pressure first-principles molecular dynamics simulations', Molecular Simulation, 28: 3, 249 — 271
**To link to this Article: DOI:** 10.1080/08927020290014367
**URL:** http://dx.doi.org/10.1080/08927020290014367

*Molecular Simulation*, 2002, Vol. 28(3), pp. 249–271



# EXAMINATION OF STRUCTURAL STABILITY AND PHASE TRANSITIONS IN CONSTANT-PRESSURE FIRST-PRINCIPLES MOLECULAR DYNAMICS SIMULATIONS

TETSUYA MORISHITA* and SHUICHI NOSÉ

*Department of Physics, Faculty of Science and Technology, Keio University, 3-14-1 Hiyoshi, Kohoku-ku, Yokohama, 223-8522 Japan*

*(Received February 2001; accepted March 2001)*



Constant-pressure first-principles molecular dynamics (FPMD) simulation is a powerful tool for investigations of structures in crystals. However, it needs enourmous computations so that highly accurate calculations for electronic states cannot be employed at present. In this report, we examined the reliability and applicability of constant-pressure FPMD in the study of structural properties under this limitation. Crystalline silicon was employed as a benchmark to perform constant-pressure FPMD simulations (with a deformable simulation cell). It is found that, in high pressure (metallic) phases, crystalline symmetry is broken with the present simulation conditions. Several structural transformations were realized by compression and decompression, but they are not entirely consistent with experiment. We discuss this discrepancy and conclude that the number of **k** point sampling in the Brillouin zone is crucial. It is recommended that constant-pressure FPMD is employed to explore candidate structures for unknown solid phases at present computational resources.

*Keywords*: First-principles; Molecular dynamics; Structural transformation; High pressure

## 1. INTRODUCTION

Structural stability and phase transitions in crystal have been studied intensively by molecular dynamics (MD) simulations since Parrinello and

*Address for correspondence: Computational Science Division, RIKEN (The Institute of Physical and Chemical Research), WAKO, SAITAMA 351-0198, Japan. Tel.: 81-48-467-9416, Fax: 81-48-467-4078, e-mail: tetsuya@atlas.riken.go.jp

ISSN: 0892-7022  DOI: 10.1080/08927020290014367

Rahman [1] introduced a modified scheme of the Andersen's constant-pressure method [2]. It is essential for dealing with structural transformations that the shape of a simulation unit cell can vary according to external pressure or temperature [1, 3]. Employing this variable cell shape formulation, structural phase transitions from one structure to another can be realized during MD runs. Many investigations of structural properties have been carried out for various types of crystals in classical MD [4–6].

In first-principles MD (FPMD) [7–9] in which electronic states are explicitly treated, we can also study structural stability and phase transitions of various materials which are not suitable for classical MD to deal with. However, it demands enormous computational resources. In FPMD, electronic wave functions are usually expressed by a plane wave basis set and matrix elements of energy are expressed as functions of reciprocal vectors. When the shape of a simulation cell varies, recalculations of reciprocal vectors and quantities depending on them are necessary at every time step. This increases computing time considerably so that FPMD with the variable cell shape (constant-pressure FPMD) is not easily carried out. Consequently, high accuracy of electronic state calculations cannot be realized and this may reduce the reliability of structural properties in constant-pressure FPMD. Although several constant-pressure FPMD simulations of structural transformations are performed recently [10–12], structural parameters and stability in crystal are not intensively studied so far, especially for metallic substance.

In this study, we report the reliability of the constant-pressure FPMD focusing on structural stability and phase transitions in crystal which are sensitive to the accuracy of electronic state calculations. With very high accurate electronic state calculations, such as large number of $\mathbf{k}$ points sampling in the Brillouin zone (BZ) and large cutoff energy for a plane wave basis set, structural properties are expected to be very close to experimental results. However, computational resources are limited especially in constant-pressure FPMD so that the accuracy of electronic state calculations should be reduced at present (*e.g.*, single $\mathbf{k}$ point sampling in the BZ with $\sim 100$ atoms). We place emphasis on detailed study of structural parameters and phase transitions under the limited accuracy of electronic state calculations and show how they behave in constant-pressure FPMD. With pressure changes, several structural transformations were realized in our simulations by both compression and decompression. However, they are not entirely consistent with experiment. We will discuss this discrepancy by comparing enthalpy of each structure.

To study several aspects of constant-pressure FPMD, we employ crystalline silicon as a benchmark. Crystalline silicon is a typical material

which has various structures according to pressure and/or temperature [13]. The diamond structure is stable at room temperature and atmospheric pressure, while at higher pressure, many other structures are observed in experiment. At 11 GPa, the diamond structure changes to the $\beta$-tin structure and at 16 GPa, $\beta$-tin changes to the simple hexagonal (sh) structure. The hcp and fcc structures are observed at higher than 40 GPa and 80 GPa, respectively. Silicon is a suitable material to examine the constant-pressure FPMD method in the study of structural stability and phase transitions. Simulations were carried out in 8 or 64 Si atom systems. In the 8 Si system, detailed structure of the diamond, $\beta$-tin, and sh were investigated with 8 $\mathbf{k}$ points sampling in the BZ. In the 64 Si system, simulations with structural transformations were carried out with $\Gamma$ point sampling in the BZ. The sampling points in the BZ are exactly the same in both systems and the cutoff energy $E_{\text{cut}}$ is taken to be 12 or 20 Ry. These values for electronic state calculations are often used in standard (fixed cell) FPMD simulations. We will show how properties of crystalline Si are observed with the accuracy of electronic state calculations described above in constant-pressure FPMD. It is also important to investigate the effect of much higher accurate electronic state calculations on structural properties. It will be reported in a forthcoming paper [14].

This paper contains following sections. In Section 2, a brief review of our computational method is described. The results of the crystal stability and simulations with phase transitions are presented in Section 3. Finally, our conclusion is described in Section 4.



## 2. CONSTANT-PRESSURE FPMD

To study structural stability and phase transitions at finite temperature in first-principles calculations, the combination of the Car-Parrinello (CP) method [7] and the Parrinello-Rahman (PR) method [1] is essential. In the CP method, the electronic states are explicitly taken into consideration and calculated within the density functional theory (DFT). Interatomic forces are given by the Hellmann-Feynman theorem in the Born-Oppenheimer (BO) adiabatic approximation. The PR method is a constant-pressure MD scheme which is often used in classical MD simulations to deal with structural transformations. In this method, changes of the shape of a simulation unit cell are allowed and three edge vectors of a unit cell are regarded as dynamical variables in addition to ionic scaled coordinates (see below). The combination of above two methods is often referred to as the constant-pressure FPMD method [10].

In this scheme, coordinates and velocities of particles are expressed in scaled forms,

$$\mathbf{R}_I = \mathbf{h}_1 s_{Ix} + \mathbf{h}_2 s_{Iy} + \mathbf{h}_3 s_{Iz} = \underline{h} s_I, \tag{1}$$

$$\mathbf{v}_I = \underline{h}\dot{\mathbf{s}}_I, \tag{2}$$

where $\mathbf{R}_I$ is a real coordinate of particle $I$, $\mathbf{s}_I$ is a scaled coordinate $(0 \le s_{Ix}, s_{Iy}, s_{Iz} \le 1)$, $\underline{h} = \{\mathbf{h}_1, \mathbf{h}_2, \mathbf{h}_3\}$ is a matrix which consists of three edge vectors of a simulation cell $\mathbf{h}_1$, $\mathbf{h}_2$, $\mathbf{h}_3$, and $\mathbf{v}_I$ is a real velocity. Single electron orbitals are also expressed in a similar scaling relation,

$$\psi_i(\mathbf{r}) = \frac{1}{\sqrt{V}} \varphi_i(\underline{h}\mathbf{s}), \tag{3}$$

where $V$ is a volume of the simulation unit cell and can be expressed as $V = \det\underline{h}$. Employing these relations, the Lagrangian of the constant-pressure FPMD method is given as

$$\begin{aligned} L = & \sum_i \mu \int |\dot{\varphi}_i|^2 d\mathbf{s} + \frac{1}{2}\sum_I M_I \dot{\mathbf{s}}_I^t \underline{h}^t \underline{h} \dot{\mathbf{s}}_I \\ & - E[\{\varphi_i\}, \{\underline{h}\mathbf{s}_I\}] + \sum_i \sum_j \varepsilon_{ij} \left( \int \varphi_i^* \varphi_j d\mathbf{s} - \delta_{ij} \right) \\ & + \frac{1}{2} W \mathrm{Tr}(\dot{\underline{h}}^t \dot{\underline{h}}) - P_{\mathrm{ex}} V, \end{aligned} \tag{4}$$

where $\underline{h}^t$ is a transposed matrix of $\underline{h}$. The first term of this Lagrangian is a fictitious classical mechanical kinetic energy of $\{\varphi_i\}$ and $\mu$ is a mass associated with $\{\varphi_i\}$. The second term is an ionic kinetic energy and the fifth term is that of $\underline{h}$, where $W$ is a mass associated with $\underline{h}$. The quantity $E$ is the sum of the total electronic energy and the ion-ion Coulomb interaction energy. Lagrangian multipliers $\varepsilon_{ij}$ are introduced to satisfy the orthonormality constraints on $\{\varphi_i\}$. The last term is related to the potential energy of $\underline{h}$ ($P_{\mathrm{ex}}$ denotes external pressure: see Ref. [10] for detail). From this Lagrangian, equations of motion for $\varphi_i$, $\mathbf{s}_I$, and $h_{ij}$ are derived as

$$\mu \ddot{\varphi}_i(\mathbf{r}) = -\frac{\delta E}{\delta \varphi_i^*(\mathbf{r})} + \sum_j \varepsilon_{ij} \varphi_j(\mathbf{r}), \tag{5}$$

$$M_I \ddot{\mathbf{s}}_I = -\underline{G}^{-1} \frac{\partial E}{\partial \mathbf{s}_I} - M_I \underline{G}^{-1} \dot{\underline{G}} \dot{\mathbf{s}}_I, \tag{6}$$

$$W \ddot{h}_{ij} = (\underline{\Pi} - P_{\mathrm{ex}}) \underline{\sigma}, \tag{7}$$

where

$$\underline{G} = \underline{h}^t \underline{h}, \tag{8}$$

$$\underline{\Pi} = \frac{1}{V}\left(\sum_I M_I \mathbf{v}_I \mathbf{v}_I - \frac{\partial E}{\partial \underline{h}} \underline{h}^t\right), \tag{9}$$

and

$$\underline{\sigma} = \frac{\partial V}{\partial \underline{h}} = V(\underline{h}^t)^{-1}. \tag{10}$$

The first term of stress tensor $\underline{\Pi}$ is a dyadic tensor. The average of diagonal elements of $\underline{\Pi}$ gives the pressure from the virial theorem. From these equations, time evolutions of $\mathbf{s}_I$ and $h_{ij}$ are determined in the same manner as the PR method and those of $\{\varphi_i\}$ are determined by formally the same equations in the CP method. Integrating these equations, FPMD under a constant-pressure condition can be implemented as far as $\{\varphi_i\}$ are kept close to the BO trajectory.

In our calculations, simulation cells containing 8 or 64 Si atoms were employed with periodic boundary conditions. Wave functions for occupied valence states were expanded in a plane wave basis with cutoff energy 12 Ry or 20 Ry. The same basis set is used during a simulation run even if drastic structural changes occur except in calculations of enthalpy (see Sec. 3.3). The number of $\mathbf{k}$ point sampling in the BZ of the simulation cell is 8 ($2 \times 2 \times 2$ for MD cell) in the 8 Si system and 1 ($\Gamma$ point) in the 64 Si system. The accuracy of our electronic state calculations is approximately the same as that in the former constant-pressure FPMD simulations of silicon [10] (*e.g.*, 54 atoms with sampling only $\Gamma$ point in BZ). The electron-ion interaction is described by a norm-conserving pseudopotential [15] with a separable form [16]. The exchange-correlation energy is described in the local density approximation (LDA) and a parameterized form by Perdew and Zunger [17] was used. The integration of equations was performed by a repetitive Verlet algorithm with a time step of 5 a.u. ($1.26 \times 10^{-16}$ s). The fictitious mass $\mu$ for $\{\varphi_i\}$ was taken to be 500 a.u., $W$ for $\underline{h}$ to be 60000 a.u., while physical mass for Si atom was used. In the simulations of structural phase transitions induced by pressure changes, we introduced two Nosé-Hoover thermostats [18–20] connected to ionic and electronic systems, respectively [21]. High pressure phases of Si are considered metallic and a large heat transfer occurs between ionic and electronic degrees of freedom [22]. Thus, thermostats are necessary to prevent large deviations of $\{\varphi_i\}$

from the BO surface during MD runs. The temperature of the ionic system is kept at 300 K while that of the electronic system very low. During simulations with thermostats, periodic resetting of the total ionic momentum was performed to suppress the ionic flow due to thermostats [23].

## 3. RESULTS AND DISCUSSION

### 3.1. Stability of Three Structures

With the variable cell shape, we examined the stability of three representative structures of Si, the diamond, $\beta$-tin, and simple hexagonal (sh) structures, in the 8 Si system. Starting from experimental lattice constants in each structure, ions, wave functions, and MD cell vectors were relaxed simultaneously in dynamical simulations. During the simulations, kinetic energies of ions, wave functions, and MD cell vectors were reduced to obtain stable structures at 0 K. External pressure $P_{ex}$ was kept at 0 GPa for diamond, 12 GPa for $\beta$-tin, and 50 GPa for sh, which are consistent values with experimental results except sh. Cutoff energy $E_{cut}$ was 12 Ry except sh, for which it was 20 Ry. For $\beta$-tin and sh, tetragonal and orthorhombic unit cells were employed, respectively, while for diamond, a cubic cell related to a conventional fcc unit cell was used. The tetragonal cell includes two conventional $\beta$-tin unit cells (see Fig. 1) stacked along c axis and the orthorhombic cell for sh includes two hexagonal layers containing four atoms each. In the calculation employing this orthorhombic cell, the sh structure was not stable lower than about 40 GPa so that higher pressure and larger $E_{cut}$ were employed to study this structure. It should be also noted that in the 8 Si sytem with sampling $\Gamma$ point only in the BZ, even the diamond structure could not keep its structure.

It is found that each of the three structures could be at least locally stable, but structures in metallic phases, $\beta$-tin and sh, converged to slightly deformed shapes after relaxations. Lattice parameters of the three structures are given in Table I. Although the lattice constant of diamond is slightly shorter than the experimental value [13], angles between cell vectors do not deviate from the ideal value (90°) and the cubic symmetry is maintained. However, for $\beta$-tin and sh, deviations of angles in few degrees and of crystalline symmetries are found. In $\beta$-tin, the ratio c/a is larger than the experimental data (lattice constant a is shorter but c is longer) and angle $\alpha$ (see Fig. 1) is $1 \sim 2$ degrees smaller than 90°. In sh, hexagonal layers are elongated along y direction (lattice constant b is 14% longer than a) and the

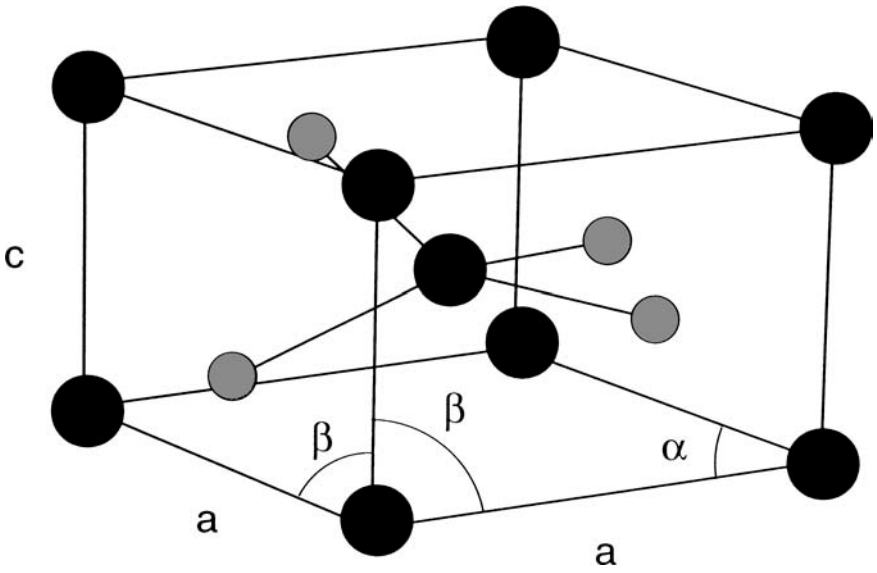


FIGURE 1 The $\beta$-tin structure at 0 K obtained by simulated annealing. The angle $\alpha$ is $1 \sim 2$ degrees smaller than 90°, while the angle $\beta$ is exactly 90°.

TABLE I Lattice parameters of three typical structures of silicon (Experimental data are quoted from Ref. [13])

| | *diamond* (0 *GPa*) | *β-tin* (12 *GPa*) | *sh* (*d-shI*) (50 *GPa*) |
|---|---|---|---|
| a/Å | 5.40 | 4.46 | 2.41 |
| (Exp./Å) | 5.44 | 4.96 (11.3 GPa) | 2.55 ( ~ 16 GPa) |
| b/Å | | | 2.77 |
| c/Å | | 2.91 | 2.17 |
| (Exp./Å) | | 2.58 (11.3 GPa) | 2.39 ( ~ 16 GPa) |
| c/a | | 0.65 | 0.90 |
| (Exp.) | | 0.55 (11.3 GPa) | 0.94 ( ~ 16 GPa) |
| $\alpha$/degree | 90.00 | 88.44 | 54.96 |
| $\beta$/degree | | 90.00 | 70.08 |
| $\gamma$/degree | | | 72.02 |
| $\varphi$/degree | | | 84.62 |

stacking is deformed. Schematic figures of this structure are given in Figure 2.

In general, these deformations are easily caused by biased sampling of reciprocal vectors **G** which are related to a plane wave basis set. In FPMD simulations, reciprocal vectors with $1/2|\mathbf{k}+\mathbf{G}| \leq E_{\text{cut}}$ are only used so that the number of **G** (plane waves) is different at each **k** point. However, if the same set of **G** vectors (for example, determined by $1/2|\mathbf{G}| \leq E_{\text{cut}}$) is used at

all **k** points except Γ point, points which satisfy the condition, $1/2|\mathbf{k}+\mathbf{G}| \leq E_{\text{cut}}$, in the reciprocal space does not distribute spherically and that results in biased sampling. In this case, slight deviations in crystalline symmetry emerge even in the diamond structure. We found that the cubic cell of diamond is deformed with 90.03 degrees in the above condition.

However, in the present simulations, above biased sampling is excluded. Another possibility is the number of **k** point sampling. From many previous electronic state calculations [24, 25], it is found that, in metallic states, a larger number of **k** points are necessary to obtain fully converged electronic

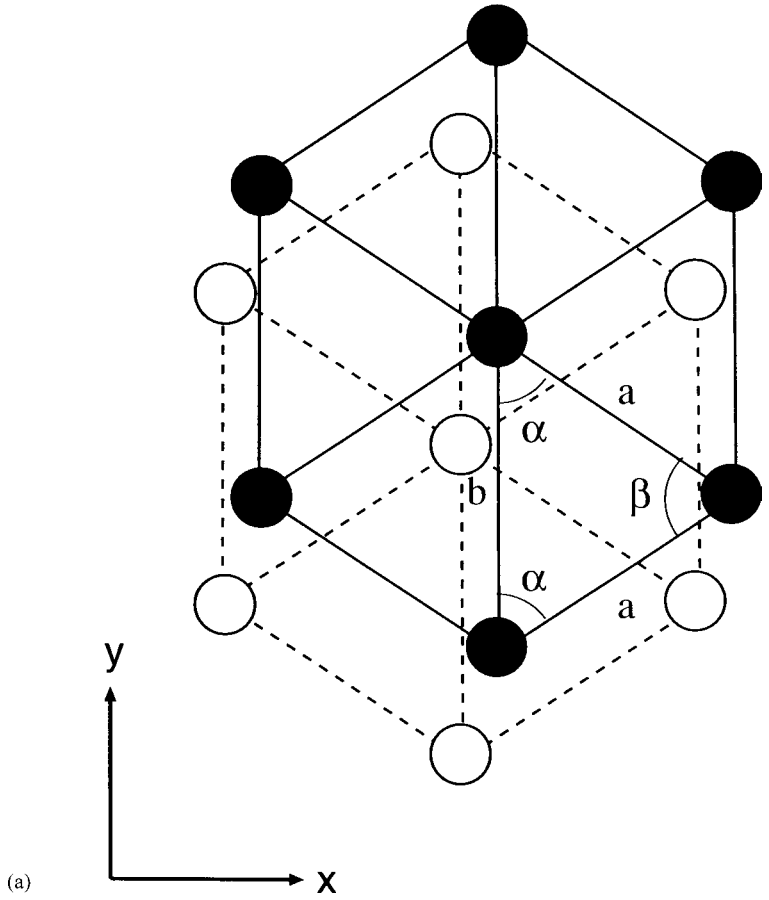


FIGURE 2 The deformed sh structure at 0 K obtained by simulated annealing. (a) Projection of hexagonal layers. The lattice parameter b is slightly longer than a. (b), (c) Projections viewed from x and y directions, respectively. The values of parameters $\gamma$ and $\varphi$ are listed in Table I.

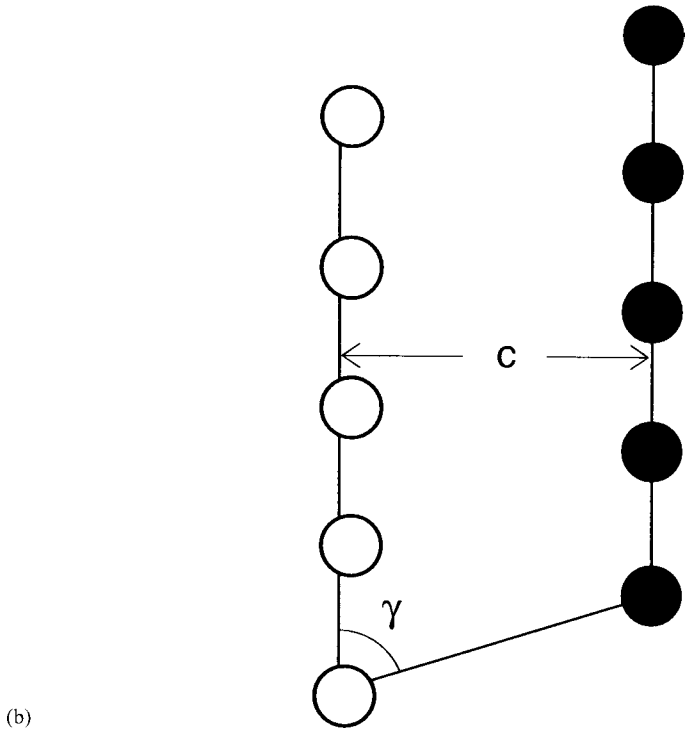


FIGURE 2 (Continued).

ground state than in semiconductor or insulator. In fact, deformations are observed only in metallic phases in our simulations. Therefore, it seems to be important to investigate the effect of the number of **k** point sampling in the BZ. Our group has investigated this effect and found that the deviations in

crystalline symmetry and lattice parameters are reduced with the large number of **k** point sampling in the $\beta$-tin and sh structures. Detailed studies on this problem will be reported in a forthcoming paper [14].

### 3.2. Structural Phase Transitions

We carried out simulations of structural transformations with pressure changes in the 64 Si system. Three transition sequences are shown: two include compression processes and one includes a decompression process.

#### *3.2.1. Compression Process I (0 GPa → 14 GPa → 26 GPa)*

A simulation accompanying a compression process was started with the diamond structure. The initial MD cell is a cube consisting of 8 conventional diamond unit cells, while in a previous study by Focher *et al.* [10], a rhombohedral MD cell containing 54 atoms was employed for diamond. External pressure was set to 0 GPa and $E_{\text{cut}}$ was to 20 Ry. At this pressure, we confirmed that the diamond structure was kept stable in our system. After equilibration in the diamond structure, pressure was raised to 14 GPa instantaneously. In experiment, a phase transition from the diamond to $\beta$-tin structures occurs around this pressure. However, no structural change was observed during the simulation. After $\sim$1ps from this compression, pressure was again raised up to 26 GPa. At the moment, the shape of the simulation cell began to change and a structural phase transition occurred. The time evolution of cell vectors $\{\mathbf{h}_1, \mathbf{h}_2, \mathbf{h}_3\}$ is shown in Figure 3. Pressure was changed at time step 5000. Lengths of cell vectors and angles between them changed largely and the MD cell converged to a shape different from the initial one within 5000 steps. We analyzed the transformed structure and found that it is almost the sh structure, but it contains a defect. The radial distribution function g(r) for this structure was calculated and this reveals clearly a characteristic feature of the sh structure. g(r) for the diamond structure (before compression) and for the transformed structure (after compression) are shown in Figure 4. Peak positions expected in an ideal sh are indicated by short bars. We can recognize small deviations from an ideal sh structure in g(r) (*e.g.*, a shoulder at 5.3 a.u.). These are caused by a defect found in detailed structural analyses. One particle is superfluous to form an ideal sh in our simulation cell, and is located within a hexagonal layer accompanying a distortion around the particle. Figure 5 shows the projection of two hexagonal layers: one layer (filled circles) contains a

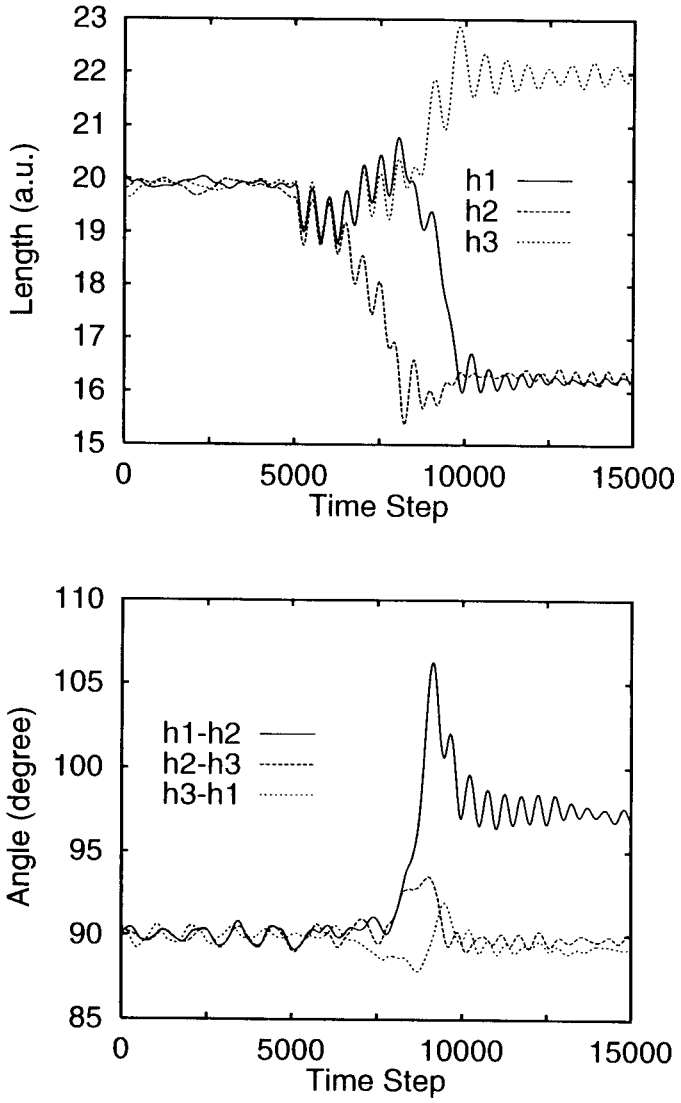


FIGURE 3 Time evolution of lengths of cell vectors (upper panel) and angles between them (lower panel) in the compression process I. External pressure was raised up to 26 GPa from 14 GPa at time step 5000. Before the compression, the simulation cell kept a cubic shape (the diamond structure) but after that, the cell shape was deformed largely and a structural transformation occurred.

superfluous particle (indicated by an arrow) which results in an interstitial defect and open circles indicate a neighboring layer. We also observed sh structures containing different types of defects in other MD runs.

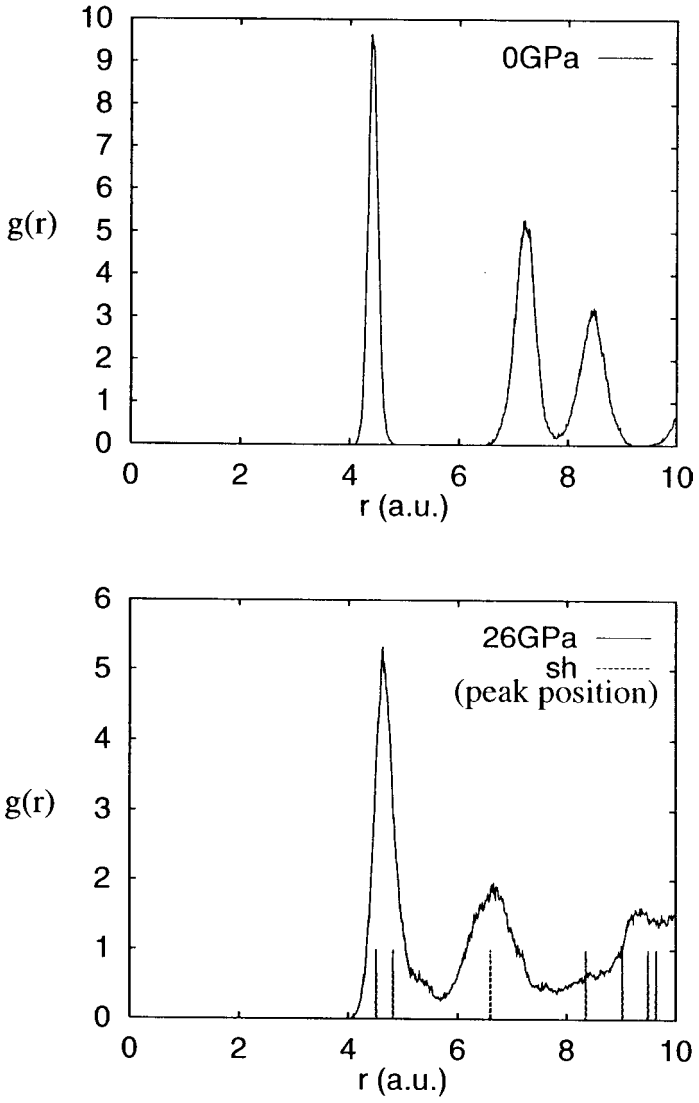


FIGURE 4 The radial distribution functions g(r) at 0 GPa in diamond (upper panel), and at 26 GPa in the transformed structure (lower panel) are shown, respectively. Peak positions expected from an ideal sh structure are shown by short bars.

We tried to recover an ideal sh structure by excluding the defect particle. We rearranged the basis set of wave functions to satisfy the condition $E_{\text{cut}} = 20$ Ry in the transformed simulation cell, and restarted the simulation at 300 K with 63 atoms after taking away the defect. In this MD run, the ionic configuration relaxed to a nearly ideal sh structure, although the

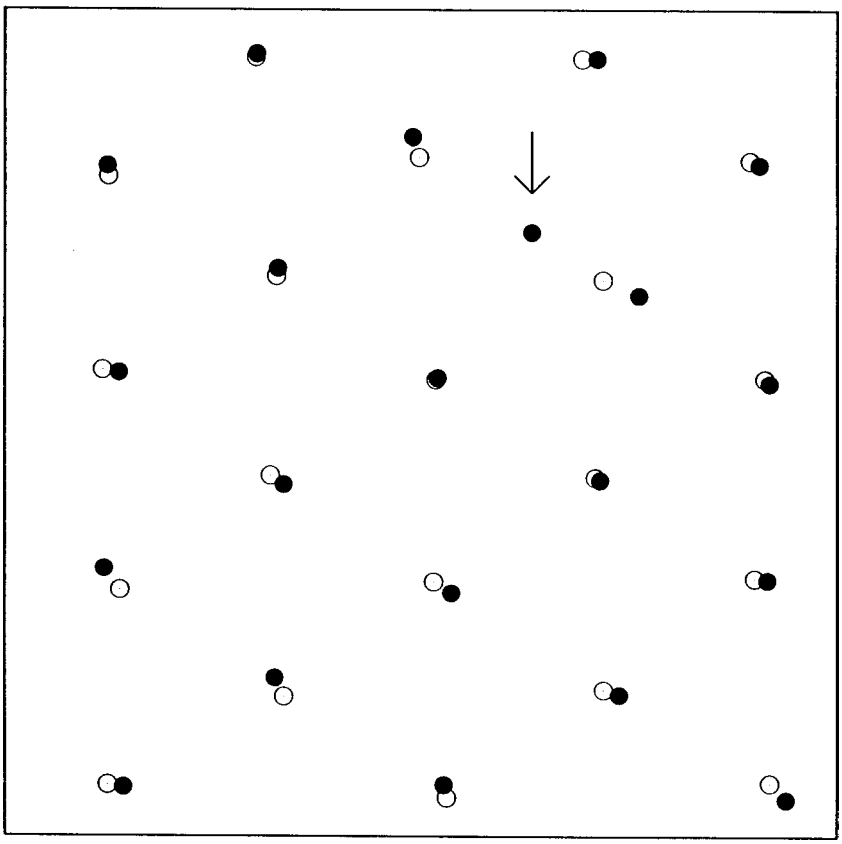

FIGURE 5 A projection of two hexagonal layers found in the sh structure transformed from the diamond structure. One layer (filled circles) contains a superfluous particle (indicated by an arrow) as an interstitial defect. Open circles indicate a neighboring layer.

stacking of hexagonal layers is slightly distorted in the same fashion as our previous study in the 8 Si system. Lattice parameters are $a = 2.55$ Å (the intralayer bond length) and $c = 2.50$ Å (the interlayer distance). A projection of three hexagonal layers is given in Figure 6. The particles are stacked accompanying a small displacement: the c axis which should be perpendicular to layers is leaned $\sim 1°$. The total energy of this structure (63 atoms) is lower about 2.5 mRy/atom than the original structure (64 atoms). This defect energy cost is quite similar to that reported by Focher *et al.* [10].

We continued the simulation with 64 atoms after the structural transformation at 26 GPa. After equilibration, we again raised pressure up to 60 GPa. At the moment, the shape of the simulation cell began to change and finally, the sh structure with an interstitial defect was transformed to the bcc structure containing grain boundaries. On the contrary, sh was

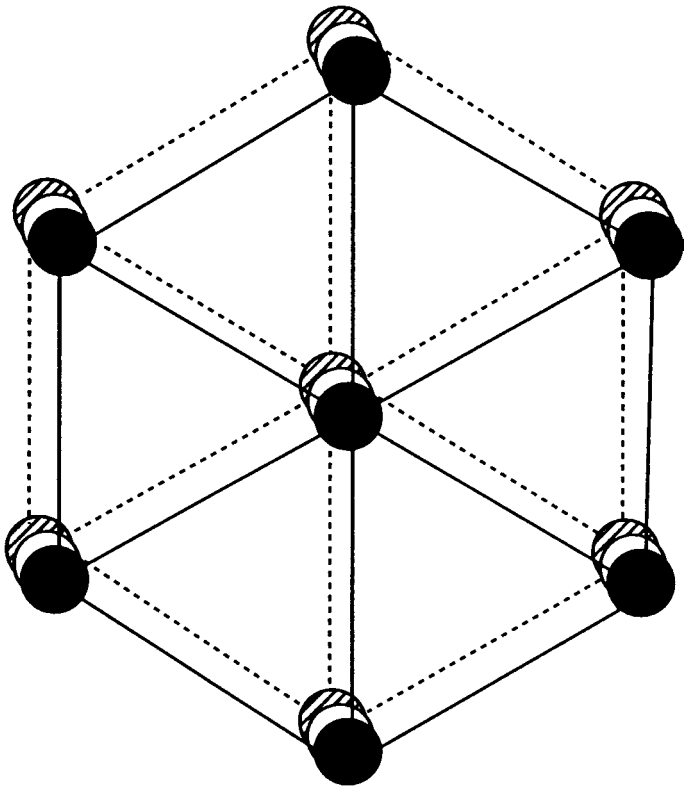

FIGURE 6 The relaxed sh structure in a 63 atom system. A projection of three hexagonal layers (corresponding to filled, open and shaded, circles, respectively) is shown. A slight distortion is found in the stacking of layers.



maintained when pressure was raised from 26 GPa to 38 GPa. This suggests that sh will not be stable at very high pressure in our simulation conditions. We observed a direct structural transformation from diamond to bcc in another compression process. This result is described in Section 3.2.2. We note that structural transformations were not observed when pressure was raised from 14 GPa to 20 GPa (0 GPa $\rightarrow$ 14 GPa $\rightarrow$ 20 GPa); the diamond structure was still kept at 20 GPa.

### *3.2.2. Compression Process II (0 GPa $\rightarrow$ 14 GPa $\rightarrow$ 38 GPa)*

Another type of structural transformation is found in a compression process up to 38 GPa (0 GPa $\rightarrow$ 14 GPa $\rightarrow$ 38 GPa). Simulation conditions are the same as the previous compression process except $E_{\text{cut}} = 12$ Ry. We also

carried out simulations with $E_{\mathrm{cut}} = 20\,\mathrm{Ry}$. However, results were not changed substantially so that the result with $E_{\mathrm{cut}} = 12\,\mathrm{Ry}$ is only given. We started the simulation with the diamond structure at 0 GPa. When pressure was changed to 14 GPa, diamond was still kept just as the previous run. However, when pressure was raised up to 38 GPa, a drastic phase transition was observed. The time evolution of cell vectors is shown in Figure 7. External pressure was raised up from 14 GPa to 38 GPa at time step 3100. Lengths of cell vectors changed largely while angles did not so

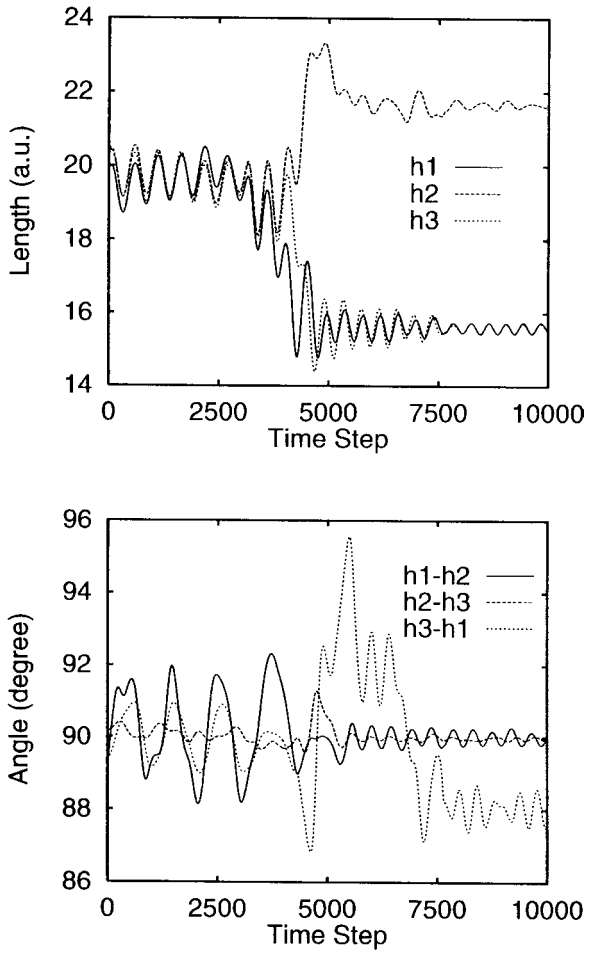


FIGURE 7 Time evolution of lengths of cell vectors (upper panel) and angles between them (lower panel) in the compression process II. External pressure was raised up to 38 GPa from 14 GPa at time step 3100. After the compression, lengths of cell vectors changed largely while angles did not so much.

much. We noticed that one angle is slightly ($\sim 2°$) deviated from 90 degrees. g(r) for the transformed structure is shown in Figure 8. This structure corresponds to the bcc structure almost perfectly. No defect exists in the transformed structure, and lattice parameter is 2.87 Å. However, one angle in the bcc cell is 88° which should be 90° in the bcc symmetry. This bcc structure is very stable in our simulations, but it is not observed in experiment at any pressure. In the former simulations by Focher *et al.* [10], the diamond structure was transformed to sh at 30 GPa but the bcc structure was not observed.

The difference between our simulations and those by Focher *et al.*, suggests that a different choice of MD simulation cell leads to different structural changes. In their simulations, a rhombohedral MD cell containing 54 atoms was employed. We note that the accuracy in their electronic state calculations is nearly the same as ours ($E_{\text{cut}} = 12$ Ry, the sampling at $\Gamma$ point only in the BZ, but we also employed $E_{\text{cut}} = 20$ Ry in some simulations). The transformation from diamond to bcc seems to be more favorable with a cubic cell than with a rhombohedral MD cell. Sampling points in the reciprocal space are different when the cell shape is different, and the stability of structures and activation energies for transitions may be also different, even with the same number of **k** points (*e.g.*, $\Gamma$ point) in the BZ. This indicates that the convergence of electronic state calculations in FPMD is not enough with respect to the number of sampling points in the BZ. Structures appearing at high pressure are considered to be metallic, and

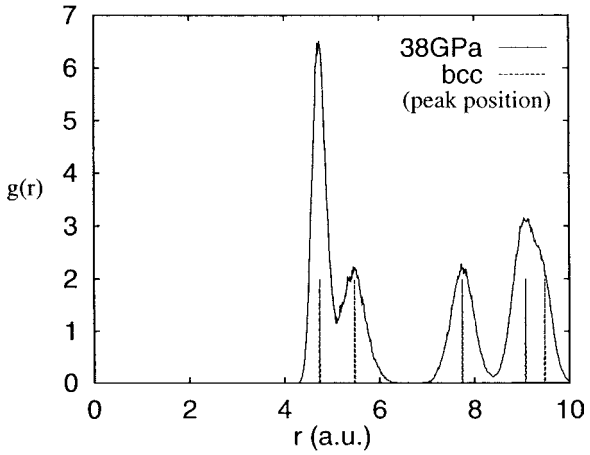


FIGURE 8 g(r) obtained at 38 GPa. Peak positions expected from an ideal bcc structure are shown by short bars.

a large number of **k** points sampling is needed to describe the Fermi surface well as described in Section 3.1. Therefore, it is inevitable that structural transformations at high pressure depend on the shape of a simulation cell in constant-pressure FPMD. The structural stability of bcc is examined comparing sh in Section 3.3.

### *3.2.3. Decompression Process (90 GPa → 38 GPa)*

We also carried out a simulation accompanying a decompression process. It started with the fcc structure at 90 GPa with $E_{\text{cut}} = 12$ Ry. The initial MD cell is a rhombohedron consisting of $4 \times 4 \times 4$ fcc primitive cells. It is confirmed that the fcc structure is stable at 90 GPa though a slight distortion was observed. After equilibration in fcc, pressure was reduced to 38 GPa instantaneously and a structural transformation was observed. In Figure 9, the time evolution of cell vectors is shown. External pressure was reduced to 38 GPa at time step 4000. Before the transition, the deviation of one angle between cell vectors ($\sim 2^\circ$) is found. It reflects a slight distortion from the fcc symmetry but it is hard to distinguish it in g(r). After decompression, a longer time was needed for equilibration than in previous compression processes. We analyzed this transformed structure and found that this is a defectless sh structure accompanying a slight distortion. g(r) for the fcc structure (before decompression) and for the transformed structure are shown in Figure 10. g(r) for the latter corresponds to sh almost perfectly, though small displacement is found in stacking of hexagonal layers (the c axis which should be perpendicular to layers is leaned $\sim 2^\circ$). Lattice parameters are $a = 2.49$ Å and $c = 2.31$ Å. The distortion is similar to that of sh obtained in Section 3.2.1 in a 63 atom system (see Fig. 6). This transition sequence is consistent with experiment and previous pseudopotential calculations, although the sh structure is locally stable at 38 GPa under the accuracy in the present study (see Sec. 3.3). It is confirmed that fcc is unstable and sh can exist (as a locally stable structure) around 38 GPa even in our crude electronic state calculations.

## 3.3. Stability of Sh and Bcc Structures

We have obtained the sh and bcc structures from the diamond structure *via* structural transformations in our simulations. To examine the stability of bcc in our simulation condition, we calculated enthalpy of the sh and bcc structures. The most stable phase under a constant-temperature and constant-pressure condition is one with the lowest Gibbs free energy.

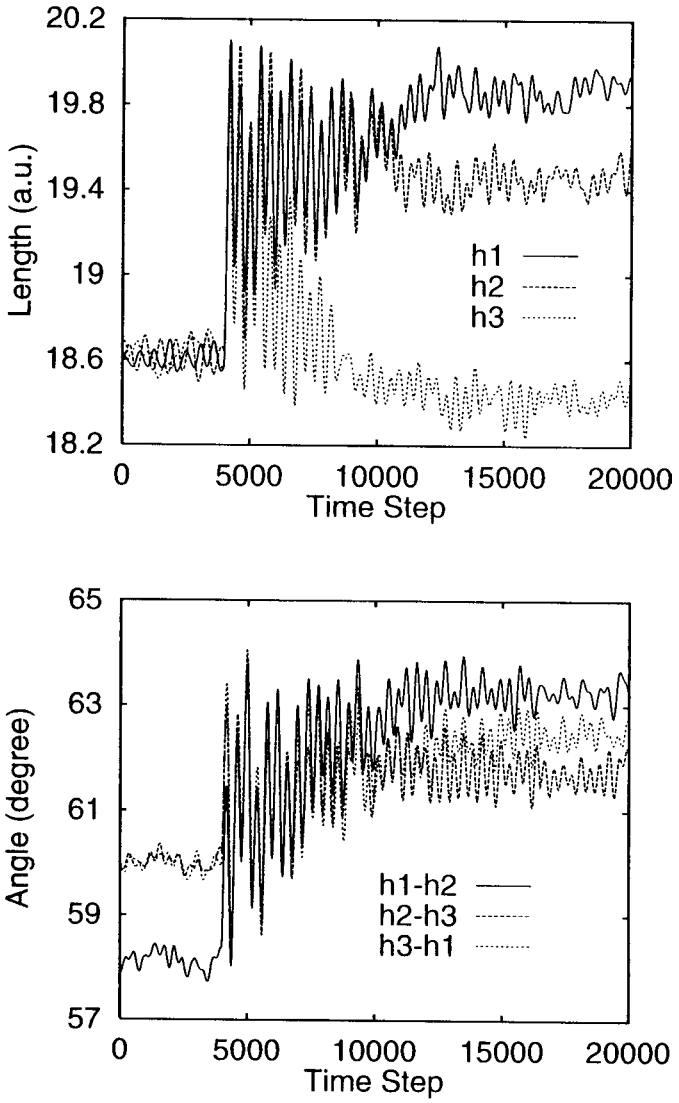


FIGURE 9 Time evolution of lengths of cell vectors (upper panel) and angles between them (lower panel) in the decompression process. External pressure was reduced at time step 4000. After the decompression, lengths of the cell vectors were elongated instantaneously. A longer time was needed for equilibration than in the compression processes.

However, it is difficult to get the Gibbs free energy accurately in MD simulations, so that we employed enthalpy as a measure of the structural stability. We assume that the entropy term is relatively unimportant in crystalline phases in a high pressure region.

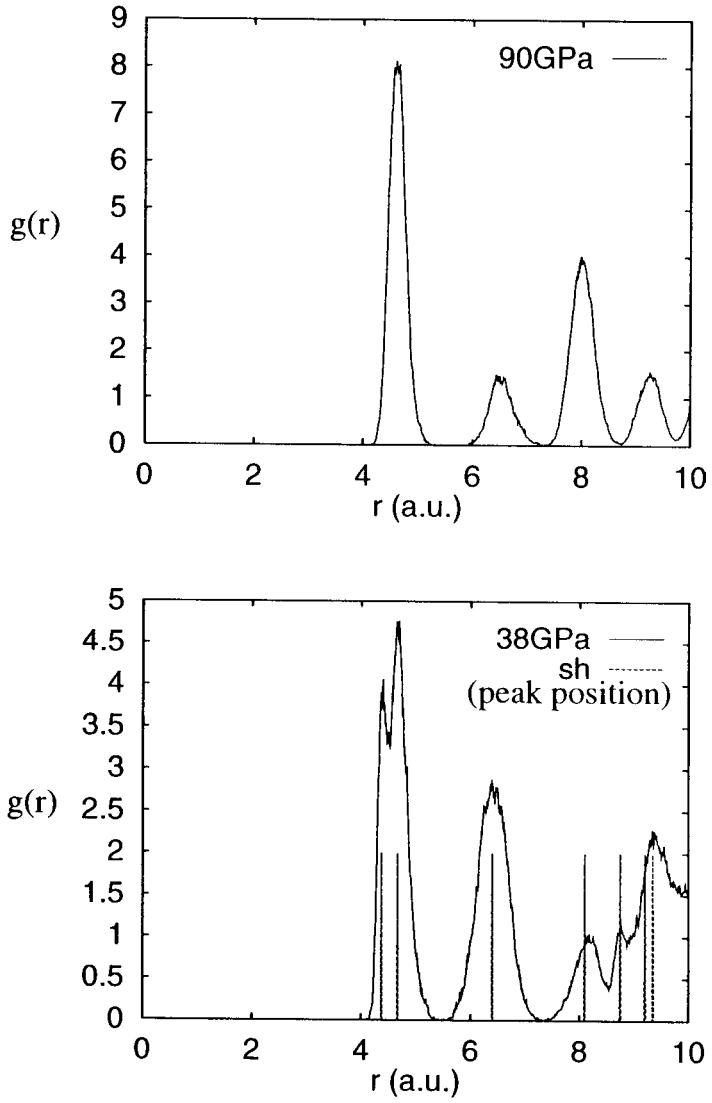


FIGURE 10 g(r) obtained in the decompression process. g(r) at 90 GPa in fcc (upper panel), and at 38 GPa in the transformed structure (lower panel) are shown, respectively. Peak positions expected from an ideal sh structure are shown by short bars.

Enthalpy was calculated for sh (the structure without any defect consisting of 63 atoms) and bcc (64 atoms) at 12, 16, 20, 26, and 38 GPa, respectively. We also tried various choices of the simulation unit cell corresponding to sh or bcc in a 64 atom system. However, configurations

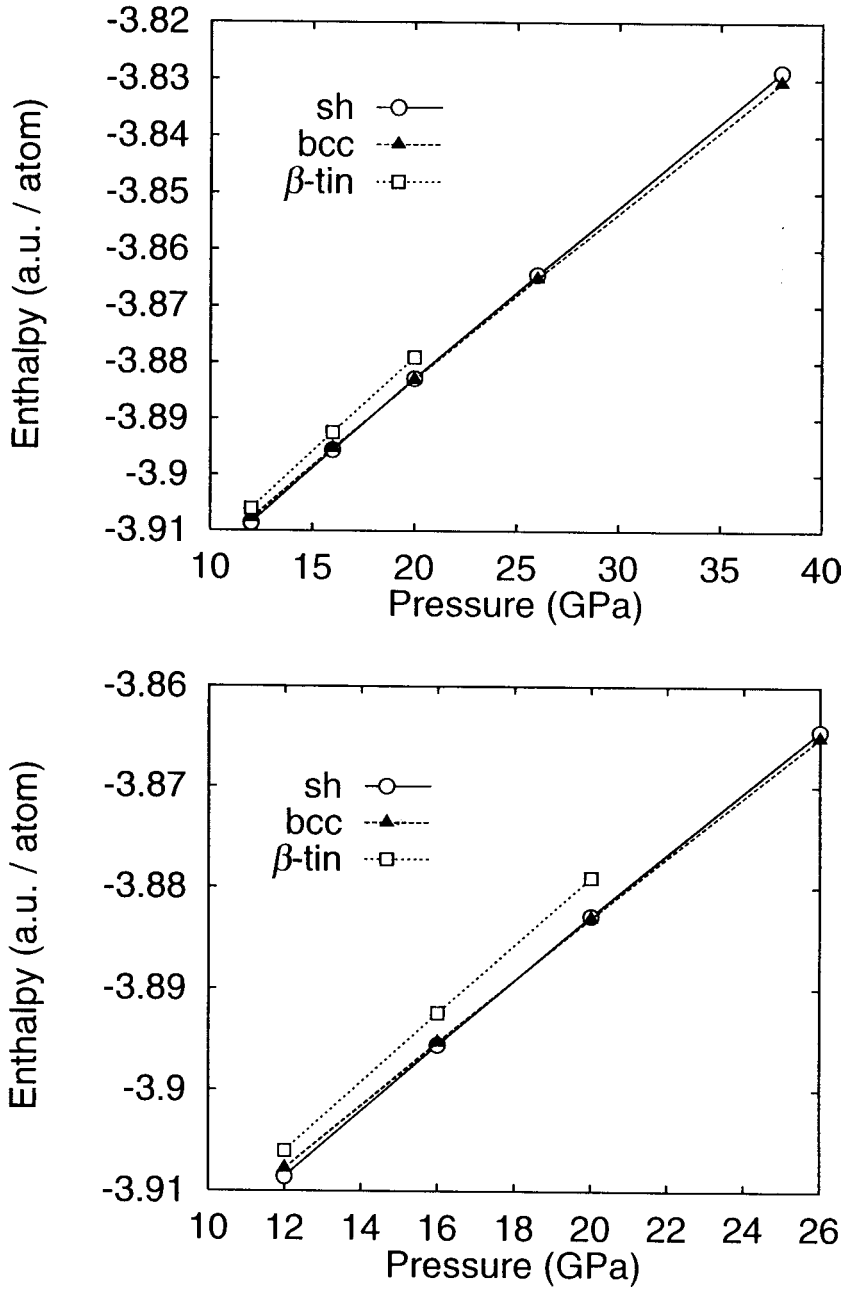


FIGURE 11 Pressure dependence of enthalpy of sh, bcc, and $\beta$-tin. In the lower panel, a magnified plot at lower pressure ($10 \sim 26$ GPa) is shown.

obtained in our compression processes give the lowest energy in both structures. It is recommended to calculate under a constant $E_{\mathrm{cut}}$ condition rather than to fix the number of plane wave basis functions, when we compare the stability of various structures with different volumes [26]. We rearranged the basis set of wave functions for each structure to satisfy $E_{\mathrm{cut}} = 20\,\mathrm{Ry}$ at a reference pressure and the same basis set was used at various pressure throughout one structure. Although these calculations were not exactly performed under a constant $E_{\mathrm{cut}}$ condition, the basis set was sampled spherically symmetric for any structures in a reciprocal space. We consider that if the spherical symmetry is satisfied, the effect caused by the deviation of $E_{\mathrm{cut}}$ from 20 Ry is negligible.

The dependence of the enthalpy on pressure is shown in Figure 11. The result of the $\beta$-tin structure at 12, 16, 20 GPa is also shown. Over $\sim 18$ GPa, bcc takes lower enthalpy while sh is more stable under $\sim 18$ GPa. Considering the structural transformation from sh to bcc (60 GPa) in our simulation (Section 3.2.1), the bcc structure will be much more stable than sh at $\sim 60$ GPa. It is confirmed that the bcc structure is definitely stable under the present accuracy over $\sim 18$ GPa. The enthalpy of $\beta$-tin is much higher than that of sh and bcc. Thus, the $\beta$-tin structure is only locally stable in our system. The enthalpy difference between sh and bcc is small (maximum difference is $\sim 0.01$ a.u. at 38 GPa). In particular, the difference at 16 and 20 GPa is about $2 \times 10^{-4}$ a.u. ($\sim 60$ K). Therefore, it is not surprising that diamond transformed to sh at 26 GPa in dynamical simulations.

The appearance of the bcc structure at 38 GPa in our simulations is considered as a result of a crude approximation in electronic state calculations employed in FPMD. The accuracy may not be enough for determining a phase diagram of crystal precisely. Therefore, the disagreement between MD simulations and experiment at high pressure is not surprising. For that reason, we consider that the sh structure observed by Focher *et al.* may not be the most stable one. However, we would like to comment that the difference is small and electronic state calculations with higher accuracy will improve the phase diagram.

## 4. CONCLUDING REMARKS

We examined the reliability of constant-pressure FPMD under the limited but widely employed accuracy of electronic state calculations in standard (fixed cell) FPMD simulations. We focused on the structural parameters

and phase transitions and found the effect of crude electronic state calculations by employing the variable cell shape. Structural parameters of solid phases of Si were investigated and symmetry breakings of crystal were found in metallic phases. Several structural transformations were realized in dynamical simulations with pressure chages but results do not entirely agree with experiment and previous psuedopotential calculations [13, 24, 25]: the bcc structure of Si is not observed in experiment and is not stable phase in whole pressure region in previous static electronic state calculations.

In our calculations, larger discrepancy between present results and experiment is found in high pressure phases, *i.e.*, metallic phases. It is reported that a huge number of **k** points sampling ($\sim$8000 in the BZ) is necessary to obtain fully converged energies for high pressure phases of Si [25]. On the contrary, we only sampled $\Gamma$ point in the BZ in the 64 Si system just as in most FPMD simulations. Therefore, it is concluded that the discrepancy between present results and experiment in structural properties is mainly due to a small number of **k** points sampling in the BZ. Considering computer resources, we cannot obtain precise structural stability in constant-pressure FPMD at present, namely, a reliable phase diagram of crystal. However, dynamical simulations often indicate more stable states and suggest transition paths when stable structures are unknown. Therefore, constant-pressure FPMD is still useful even in crystalline phases at high pressure to explore new phases.

From our simulations, it is concluded that structural transformations in constant-pressure FPMD are strongly affected by accuracy of electronic state calculations. When one study structural transformations in metallic phases, it is recommended that the constant-pressure FPMD method is employed to obtain candidate structures for unknown phases, and that static electronic state calculations with high accuracy are applied to these structures to determine phase diagrams, unless they are largely changed at different temperature. Higher accuracy of electronic state calculations will improve the applicability of the constant-pressure FPMD method.



***Acknowledgements***

The authors would like to thank N. Matsuura and I. Kato for their efforts in the preliminary study of this investigation. This work is partly supported by the Grant-in-Aid for Scientific Research from the Ministry of Education, Science, Sports and Culture. The computations were carried out at the Computer Center of the Institute for Molecular Science and at Computer Center, University of Tokyo.

## *References*


[1] Parrinello, M. and Rahman, A. (1980). "Crystal structure and pair potentials: A molecular-dynamics study", *Phys. Rev. Lett.*, **45**, 1196.

[2] Andersen, H. C. (1980). "Molecular dynamics simulations at constant pressure and/or temperature", *J. Chem. Phys.*, **72**, 2384.

[3] Wentzcovitch, R. M. (1991). "Invariant molecular-dynamics approach to structural phase transitions", *Phys. Rev. B*, **44**, 2358.

[4] Nosé, S. and Klein, M. L. (1983). "Constant pressure molecular dynamics for molecular systems", *Mol. Phys.*, **50**, 1055.

[5] Nosé, S. and Klein, M. L. (1989). "Structural and dynamics of the fluorperovskite, $RbCaF_3$", *J. Chem. Phys.*, **90**, 5005.

[6] Hashimoto, T., Sugawara, S. and Hiwatari, Y. (1996). "Structural transformations of ice at high pressures *via* molecular dynamics simulations", *Mol. Sim.*, **18**, 115.

[7] Car, R. and Parrinello, M. (1985). "Unified approach for molecular dynamics and density-functional theory", *Phys. Rev. Lett.*, **55**, 2471.

[8] Arias, T. A., Payne, M. C. and Joannopoulos, J. D. (1992). "Ab initio molecular-dynamics techniques extended to large-length-scale systems", *Phys. Rev. B*, **45**, 1538.

[9] Kresse, G. and Hafner, J. (1994). "*Ab initio* molecular-dynamics simulation of the liquid-metal-amorphous-semiconductor transition in germanium", *Phys. Rev. B*, **49**, 14251.

[10] Focher, P., Chiarotti, G. L., Bernasconi, M., Tosatti, E. and Parrinello, M. (1994). "Structural phase transformations *via* first-principles simulation", *Europhys. Lett.*, **26**, 345.

[11] Wentzcovitch, R. M. (1994). "hcp-to-bcc pressure-induced transition in Mg simulated by ab initio molecular dynamics", *Phys. Rev. B*, **50**, 10358.

[12] Bernard, S., Chiarotti, G. L., Scandolo, S. and Tosatti, E. (1998). "Decomposition and polymerization of solid carbon monoxide under pressure", *Phys. Rev. Lett.*, **81**, 2092.

[13] Hu, J. Z., Merlcle, D., Menoni, C. S. and Spain, I. L. (1986). "Crystal data for high-pressure phases of silicon", *Phys. Rev. B*, **34**, 4679.

[14] Tashiro, J., Morishita, T. and Nosé, S., *in preparation.*

[15] Bachelet, G. B., Hamann, D. R. and Schlüter, M. (1982). "Pseudopotentials that work: From H to Pu", *Phys. Rev. B*, **26**, 4199.

[16] Kleinman, L. and Bylander, D. M. (1982). "Efficacious form for model pseudopotentials", *Phys. Rev. Lett.*, **48**, 1425.

[17] Perdew, J. and Zunger, A. (1981). "Self-interaction correction to density-functional approximation for many electron systems", *Phys. Rev. B*, **23**, 5048.

[18] Nosé, S. (1984). "A unified formulation of the constant temperature molecular dynamics methods", *J. Chem. Phys.*, **81**, 511.

[19] Hoover, W. G. (1985). "Canonical dynamics: Equilibrium phase-space distributions", *Phys. Rev. A*, **31**, 1695.

[20] Nosé, S. (1986). "An extension of the canonical ensemble molecular dynamics method", *Mol. Phys.*, **57**, 187.

[21] Blöchl, P. and Parrinello, M. (1992). "Adiabaticity in first-principles molecular dynamics", *Phys. Rev. B*, **45**, 9413.

[22] Pastore, G., Smargiassi, E. and Buda, F. (1991). "Theory of ab initio molecular-dynamics calculations", *Phys. Rev. A*, **44**, 6334.

[23] Morishita, T. and Nosé, S. (1999). "Momentum conservation law in the Car-Parrinello method", *Phys. Rev. B*, **59**, 15126.

[24] Yin, M. T. and Cohen, M. L. (1982). "Theory of static structural properties, crystal stability, and phase transformations: Application to Si and Ge", *Phys. Rev. B*, **26**, 5668.

[25] Needs, R. J. and Mujica, A. (1995). "First-principles pseudopotential study of the structural phases of silicon", *Phys. Rev. B*, **51**, 9652.

[26] Dacosta, P. G., Nielsen, O. H. and Kunc, K. (1986). "Stress theorem in the determination of static equilibrium by the density functional method", *J. Phys. C*, **19**, 3163.